Measurement of Thermal Conductivity in Niobium using Pump-probe TDTR Spectroscopy

Submitted by:
Hani E. Elsayed-Ali, P.I.
Md Obidul Islam, Ph.D. student
Old Dominion University
Applied Research Center
12050 Jefferson Ave., Suite 721
Newport News, VA 23606
Phone: (757)269-5645 or (757)683-3748; Fax: (757) 269-5644
http://www.odu.edu/eng/research/enterprise-centers/arc

Abstract:

Thermal diffusion of bulk niobium and films of varying thickness deposited at different temperatures, is investigated by optical pump-probe thermo-modulation spectroscopy using a femtosecond Ti:sapphire oscillator (average power ~ 450 mW, wavelength ~ 800 nm, pulse width ~100 fs). Thermal conductivity of Nb films of thickness 800 nm, 400 nm and 200 nm is determined by curve fitting approach using 1D heat diffusion model and a little decrease in conductivity with decreasing thickness is measured. This reduction in conductivity for thin Nb films deposited at room temperature can be recovered somewhat by depositing the films at higher temperature (670^0 C). Thermal conductivity of Nb is measured a bit less with Cu used as substrate (50 $Wm^{-1}K^{-1}$) compared to the films of same thickness but with sapphire substrate (55 $Wm^{-1}K^{-1}$). Substantial and periodically distributed acoustic echoes appeared on the experimentally observed thermoreflectance signals collected from niobium films deposited on copper substrate. Using the period of acoustic oscillation, the longitudinal sound velocity inside niobium is calculated as 4395.6 ms-1, which is in good agreement with the values reported in literature. Thermal diffusion through niobium relies considerably on the thickness of the films, the substrates and the temperature at which films are deposited

1. Introduction

The heat transfer in pure Nb are attracting significant interest due to the increasing demand in particle accelerator cavity. In SRF cavity superconducting materials with comparatively higher thermal conductivity are needed because superconductors such as niobium with poor thermal conductivity exhibits thermal instability caused by local heating [1]. Such SRF resonators, built by depositing thin superconducting layer on a high conductivity, relatively low-cost supporting structure provide much better thermal stability at lower costs. Copper is a good choice for the resonator wall material for its excellent thermal stability and low cost. Although poor thermal conductivity of Nb causes thermal instability, considering the several economic and technological benefits, Nb coated copper cavities are pondered as the suitable alternative to bulk Nb for SRF applications [2].

The thermal conductivity of Nb thin film on Cu substrate plays a vital role in SRF cavity since low thermal conductivity limits the maximum accelerating gradient (cavity quench) of the cavity. One way of improving the cavity thermal conductivity is to use of high purity Nb. Thermal conductivity of Nb thin films also depend on the thickness and crystallinity of the films. In this report, thermal conductivity (k) of Nb for various film thickness has been quantified using pump-probe thermoreflectance technique and confirmed using 1D heat diffusion model. The one-dimensional heat diffusion model can be used to measure the thermal conductivity since the laser beam focal diameter (20μm) is large compared to the optical skin depth (20 nm for Nb) [3]. Absorption of the laser causes thermal expansion and generates acoustic waves of ultrasonic frequency. This strain effects on reflectivity is superimposed with the reflectance due to temporal relaxation profile. Using periodic acoustic oscillations appeared with the thermoreflectance signals and thickness of the Nb film, the longitudinal sound velocity is determined.

Time-domain thermoreflectance (TDTR) is a powerful technique for measuring the thermal diffusivity and interfacial conductance of thin films when ultrafast laser excitation occurs on metals and superconductor [4]. The electrons absorb the laser energy and become hot electrons. These hot electrons can be elevated to a significantly higher temperature than the lattice if the pulse width of the excitation laser is shorter than the electron-phonon relaxation time. A probe pulse at later times monitors the change either in transmission or reflection which can be related to the change in electron and lattice temperature. After the incident laser pulse, the high-temperature hot electrons begin to cool down by transferring their excess energy to the lattice through electron-phonon scattering. The hot electrons and lattice achieve thermal equilibrium in a time scale of less than a few picoseconds [5].

First experimental investigation of pump-probe thermo-modulation on Cu films using 8 ps laser pulse was done by Eesley in 1983 [6]. In 1987, two separate research groups Elsayed-Ali et al. and Eesley et al. pioneered the use of subpicosecond lasers to resolve nonequilibrium heating in Au and Cu [7, 8]. Alfano et al. reported on the investigation of electron-phonon relaxation time and electron-phonon coupling constant of Nb by femtosecond pump-probe experiment [5, 9, 10]. Most of the early investigations were performed on very thin films in order to observe the electron–phonon relaxation while minimizing the effects of diffusion. However, Paddock and Eesley used the TDTR technique in 1986 to measure the thermal conductivity of thin films [11]. Several

investigators have recently revisited this idea since the thermal properties of thin films have become a topic of great interest to the microelectronics industry [12].

The surface of the thin films is usually more rough than bulk metals and contain more defects in the crystalline structure. The electron-electron and electron-phonon interactions in thin metal films differ strongly from that of bulk materials [13-14]. Surface roughness depends on the deposition temperature and higher deposition temperature is responsible for sharper critical temperature transition [15]. The surface quality can be improved by epitaxial growth and minimizing grain boundary density. Therefore, both surface and superconducting parameters are crucial concern for better SRF performances.

Thermo-modulation of noble metals like Au or Cu shows three events: (i) a fast rise on the order of few hundred femto-seconds due to creation of hot-electrons by high-energy pump beam, (ii) a fast decay component on the order of few pico-seconds due to transient change in hot-electron temperature (hot electrons transfer energy to lattice). The cooling of hot electron is characterized by the term of Fermi-level smearing, and (iii) a slow decay component on the order of nano-second due to the change in lattice temperature [5]. Both free electrons and lattice play significant role in the absorption and relaxation processes involved in short-pulse laser heating. The thermal relaxation trace is convolution of both Te and Tl [3].

$$\Delta R = a\Delta T_e + b\Delta T_l \quad \text{(1)}$$

Where, a and b are functions of photon energy and the complex dielectric function. It is well established that, in the regime 300 K < T_e< 700 K, the maximum reflectivity change $(AR)_{max}$ is observed to be proportional to the laser fluence. Again, the maximum electron-temperature change $(AT_e)_{max}$ is roughly proportional to laser fluence. Therefore, $(AR)_{max}$ is also roughly proportional to $(AT_e)_{max}$. Since the electron temperature in our experiment lies within the range, the normalized electron-temperature change can be deduced from the measured reflectivity-change as the equation (9) [16]:

$$\frac{\Delta T_e}{(\Delta T_e)_{max}} = \frac{\Delta R}{(\Delta R)_{max}} \quad \text{(2)}$$

In the conventional Fourier Heat Conduction Model, the radiation energy is assumed to be converted into lattice energy instantaneously and energy transfer in solids is assumed entirely to be a diffusion process [17]. During the first few picoseconds after laser absorption, lattice temperature is small and does not play significant role. Therefore, thermal conductivity should be measured by fitting the experimental data with the theoretical heat conduction model after first few picoseconds.

2. Experimental setup

Figure 1 portrays the pump-probe experimental set-up for time domain thermoreflectance (TDTR) measurement at ODU, Applied Research Center (ARC). Tsunami Titanium: Sapphire (Ti: Al_2O_3) oscillator of center wavelength, λ= 800 nm, FWHM pulse duration, τ =100 fs and repetition rate of 80 MHz is used as laser source. The laser beam is split into intense pump and weak probe beam by a nonpolarizing beam splitter with an intensity ratio of 90:10. The intense pump beam of 1.25 nJ pulse is used as a heating source whereas the lower power probe beam is used to monitor the change in reflectivity of the sample. The pump beam is guided through an acousto-optic

modulator (IntraAction AOM-402AF3) to modulate the pump beam at a prescribed frequency of 600 kHz. A half wave plate is used to rotate the polarization of the pump relative to the probe. Next the pump beam passes through a set of two mirrors mounted on a micro-positioning stage (Newport FC100) used to vary the optical path length between pump and probe.

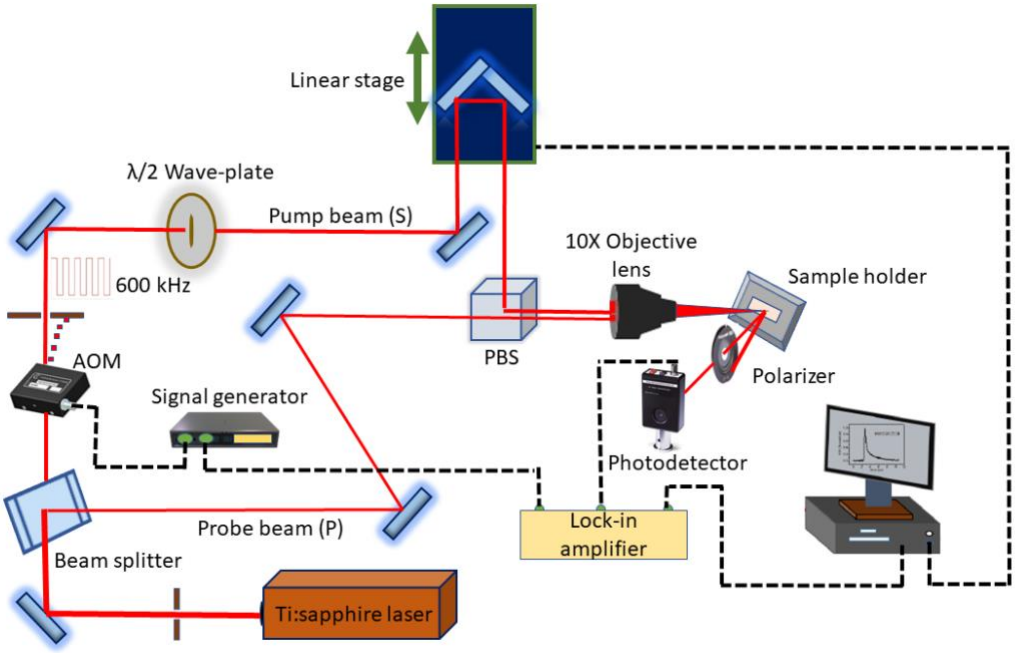

Fig. 1. Femtosecond time domain thermoreflectance pump probe setup at ARC. Acousto-optic modulator is used to modulate the pump beam at 600 kHz frequency. The linear stage is used to create the time delay between pump and probe beam.

A minimum of 6.67 fs time delay is created between the arrival of pump and probe pulses as the optical path length of the pump is varied by 1 μm. A 10X objective lens is used to focus the pump and the probe beam as diameter of 20 μm and 10 μm respectively. The probe beam is focused in an incident angle of 3^0 from normal to make the pump and probe non-colinear. The size of the pump beam is larger than the probe beam assuring that the probe beam lies entirely within the heated region. The reflected probe beam is detected by a Si photodiode detector (DET 10A). A polarizer positioned before the detector to block the effect of scattered s polarized pump beam. A lock-in amplifier (SR 865A) is used to determine the magnitude and phase of the signal at the modulation frequency of the AOM.

A LabView program is used to record transient signal (ΔR) and control the motion of the linear stage. To determine ΔR/R, the transient signal (ΔR) is divided by the static DC signal from the photodetector in the absence of pump beam. This eliminate any dependence of the final signal on the probe intensity or the size of the pinhole in front of the photodiode.

3. Thermal Conductivity Model

The femtosecond laser pulse localized the heat both spatially and temporally on the thin films. To measure the thermal properties, a relationship between the reflectance of the film and the theoretical thermal response must be known. The heated electrons and phonons alter the dielectric

constant which in turn changes the reflectivity of the sample. The change in the dielectric constant is proportional to the change in both electron and lattice temperature. Diffusion in the direction of pump beam is negligible during the time of measurement, since the sample is thin compared to the optical skin depth [9]. The parabolic one-step heat transfer model deduced from Fourier's law is given by equation (3).

$$C\frac{\partial T_{(x,t)}}{\partial t} = -k\frac{\partial^2 T_{(x,t)}}{\partial x^2}) + S(x,t) \quad \text{..... (3)}$$

Where, *T(x,t)* is the temperature profile, *x* is the distance normal to the film surface, *C* is the heat capacity per unit volume, *k* is the thermal conductivity and $S(x,t)$ is the laser source term, heat energy generated per unit volume per unit time. The laser source term has an exponential decay in space to account for absorption in a nontransparent media, and a Gaussian shape in time. Neglecting the temperature dependence of the optical properties a reasonable approximation of the source term is given by equation (4) [18-20].

$$S(x,t) = (1-R)\frac{J}{t_p d} * \exp\left[-\frac{x}{d} - 2.77(\frac{t}{t_p})^2\right] \quad \text{..... (4)}$$

Where, R is the reflectivity of the material, J is laser fluence, d is radiation penetration depth and t_p is pulse width. Here R and d are material properties and J and t_p are laser parameters. Lattice heat capacity, thermal conductivity and radiation penetration depth for bulk Nb as reported in literature are $2.3x10^6$ J/m3-K, 55 W/m-K and 20 nm respectively [5, 9]. The reflectivity (R = 0.9) is measured on the 1 µm Nb sample on sapphire substrate. The sample was placed at a very small angle (15^0) to the incident laser beams and an optical lens was used to collect the whole laser beam reflected from the sample and focus onto a photodiode detector that is placed far away from the sample so that the incident and reflected beams are almost parallel to each other. A list of parameters and values of the laser used in the pump-probe experiment at ODU Applied Research Center (ARC) is given in table 1.

Table 1: ARC Femtosecond Laser Specifications

LASER parameters	**Values**
Center Wavelength	800 nm
Repetition Rate	80 MHz
Pulse Width	100 fs
Pump Power	100 mW
Probe Power	15 mW
Focal Spot Diameter (Pump)	20 µm
Focal Spot Diameter (Probe)	10 µm
Pump Energy	1.25 nJ
Pump Fluence	3.98 Jm^{-2}
Pump laser intensity	3.98 X 10^{13} Wm^{-2}
Photon energy	1.553

The initial condition is the initial temperature which is set to the room temperature (300 K) is given by equation (5)

$$T(x,-2t_p) = T_0 \quad \text{..... (5)}$$

During the short period of laser heating, heat losses from the front and back surfaces of the film can be neglected, leading to the thermal-insulation boundary conditions:

$$\left.\frac{\partial T}{\partial x}\right|_{x=0} = \left.\frac{\partial T}{\partial x}\right|_{x=L} = 0 \quad \text{..... (6)}$$

Figure 2 shows the normalized temperature profiles obtained from 1D heat diffusion model using above source laser parameters and boundary conditions. Figure 2 (a) gives the temperature profiles for normalized full scale for conductivity k = 55 $Wm^{-1}K^{-1}$(conductivity for bulk Nb) and 2 (b) is for temperature profiles for reduced vertical scale to differentiate among three different conductivity values 55 $Wm^{-1}K^{-1}$ (solid curve), 50 $Wm^{-1}K^{-1}$ (dotted curve) and 45 $Wm^{-1}K^{-1}$ (dashed curve). The temporal resolution is taken as 0.667 ps and the horizontal scale is taken upto 900 ps (same resolution and time scale taken for experimental data acquisition).

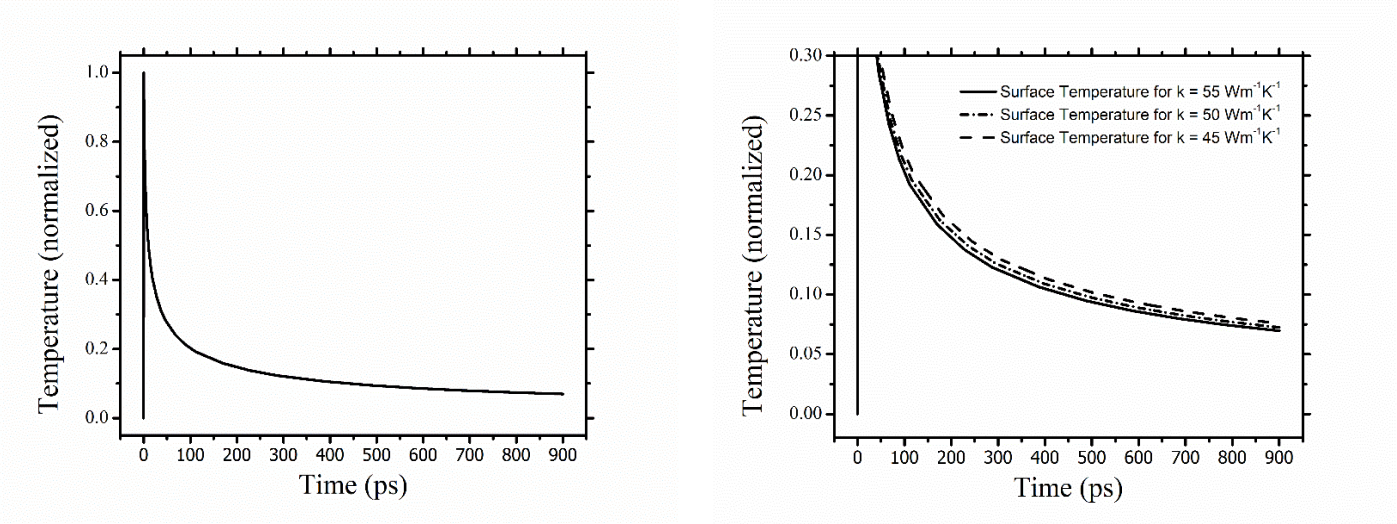

(a) **(b)**

Fig. 2. Temperature profiles obtained by 1D Fourier Heat Diffusion Model (a) temperature profile for conductivity k = 55 $Wm^{-1}K^{-1}$ (normalized full vertical scale) (b) temperature profiles for three different conductivity values k = 55, 50, 45 $Wm^{-1}K^{-1}$ (normalized reduced vertical scale)

4. Measurements in Bulk Niobium

The samples used to observe the thermoreflectance signal are well polished for pump-probe experiments. The surface of the bulk Nb sample is shown in Fig 3 where 6 different spots are marked. The transient signal (ΔR) collected from these spots were in the range of 10^{-8} V. The ΔR is divided by the static DC signal R from the photodiode which is in the range of mV to eliminate any dependence of the final signal on the intensity or size of the probe beam.

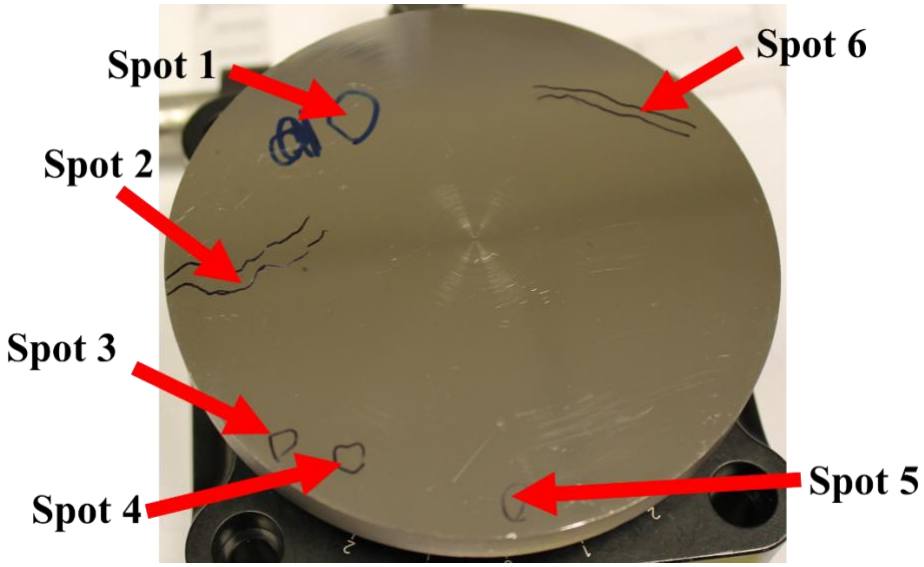

Fig. 3. Surface of the bulk Nb sample.

Figure 4(a) shows the transient signals obtained from the 6 spots and Fig. 4(b) presents the normalized ΔR/R signal fitted with 1D Heat Diffusion Model. The different scan in the same point shows approximately ± 1 W/mK variations in the conductivity as shown in Fig. 5(a) and 5(b) for 3 different scans from spots 1 and 3 respectively. The fluctuation can be removed by averaging a greater number of scans.

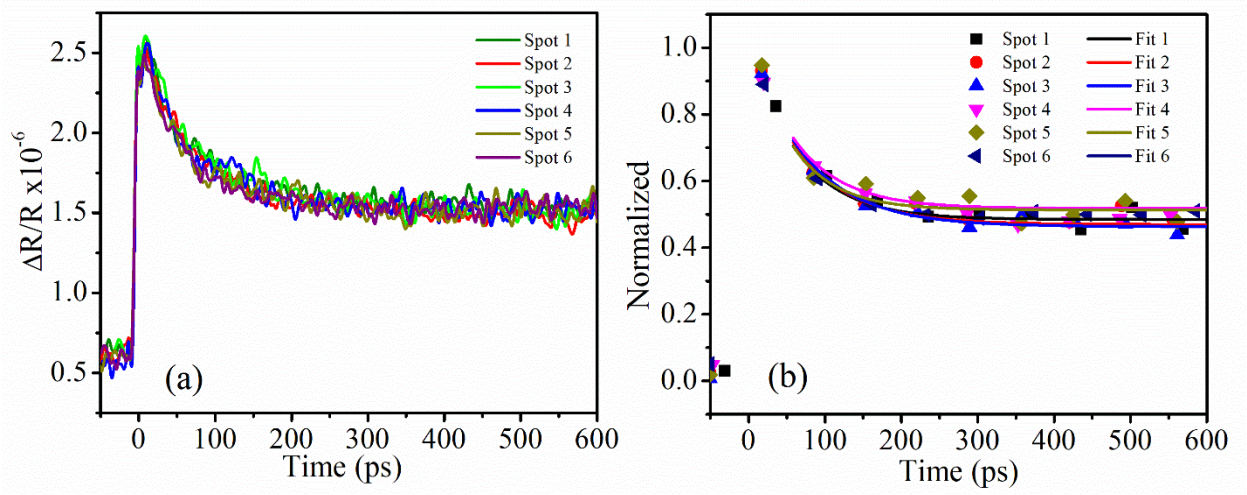

Fig. 4. (a) *ΔR/R* from different spots of the Nb surface. (b) Normalized *ΔR/R* signals from 6 different spots are fitted with 1 D heat equation.

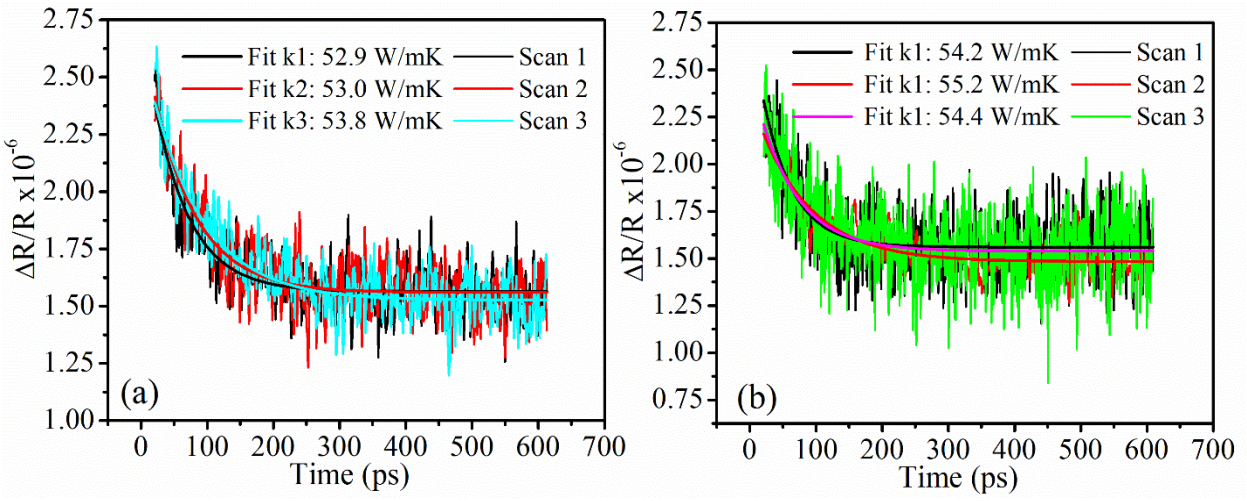

Fig. 5. (a) *ΔR/R* signal for 3 different scans from spot 1. (b) *ΔR/R* signal for 3 different scans from spot 3.

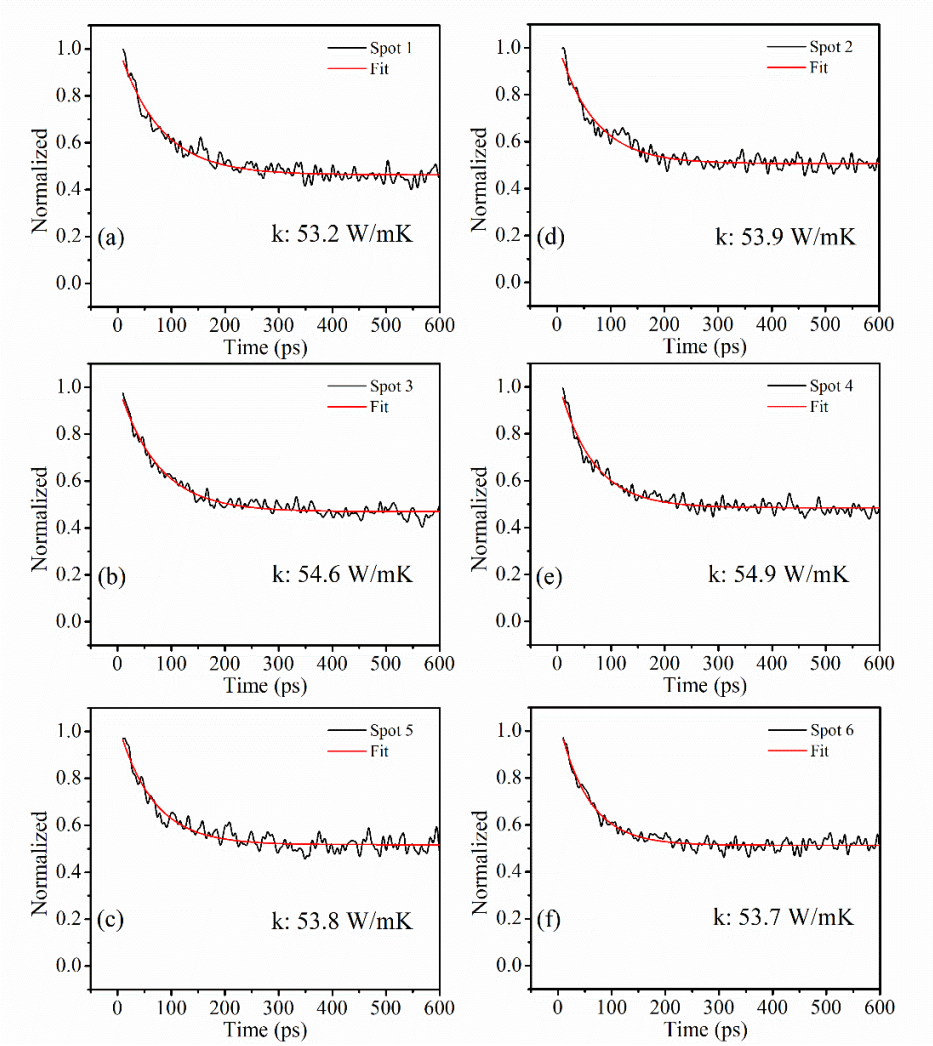

Fig. 6. Thermal conductance value of 6 different spots. Each data is average of 3 scans. The average thermal conductivity is calculated as 54.4 W/mK.

In Fig. 6, the averaged signal, collected from 3 scans is shown. The value of the fitting parameter, R- square is approximately 0.9 and the average thermal conductivity is calculated as 54.4 W/mK for the whole sample. Similar thermal conductance value was reported by different groups in their experiments. Thermal conductivity for bulk Nb was reported as 55 W/mK by Mihailidi et al. [9] and 54 W/mK by F.Koechlin et al. [21]. The error bar is included in Fig. 7 which represents the standard deviation of each data points.

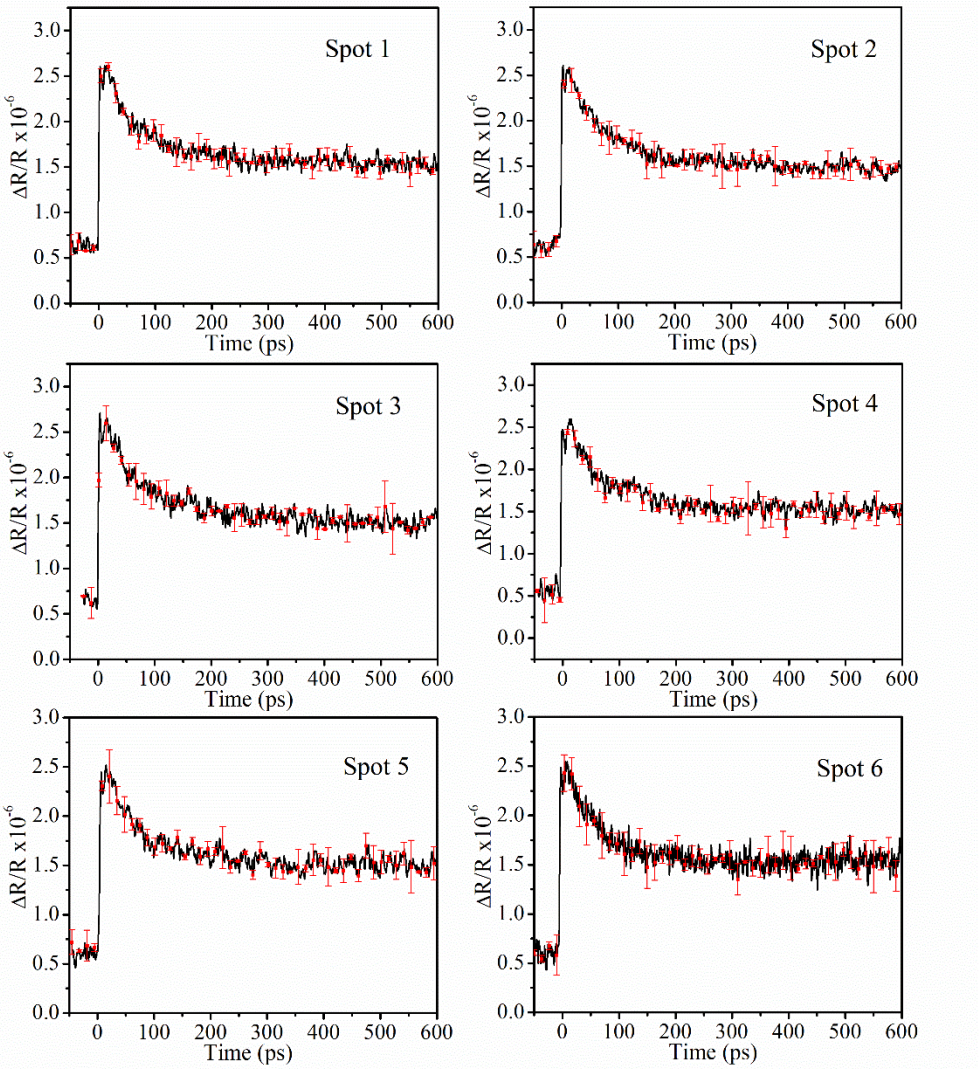

Fig. 7. The *ΔR/R* signal from different spots of the Nb sample. Each curve is the average of 3 scans. The error bar represents the standard deviation of data points.

All the scans obtained from the bulk Nb sample shown in Fig. 3 are obtained for 0-600 ps time-delay between pump and probe beam produced by a 10 cm linear translational stage. The variation of the signal in the present work can be minimized by using longer heat diffusion time scan and more accurate thermal conductivity can be measured. Later the 10 cm linear stage is replaced by a 30 cm linear stage and the time-delay has been increased and the thermoreflectance data from thin Nb films are obtained for 900 ps scan time which will be presented on the following sections.

5. Measurement in Thin Niobium Films Deposited at Room Temperature

Circular plate of Copper of diameter 2.5 cm are obtained from II-VI. Niobium films of thickness 800 nm, 400 nm and 200 nm were deposited using AJA ATC Orion 5 Magnetron sputtering system. The copper substrate and deposited Nb films are shown in Fig. 8. A 2-inch 99.999% Nb sputter target has been used for DC sputtering of Nb films. The deposition vacuum chamber was evacuated to a base pressure of low 10^{-7} Torr before deposition. The deposition was performed at 3 mTorr with an argon flow rate of 20 SCCM. The argon gas used is of very high purity (99.999%) and of grade 5n. During sputtering, the DC power applied to the sputter gun was 130 W and the deposition was done with the substrate left at room temperature. To obtain a uniformly coated film, the substrate holder was rotated at 50 rpm throughout the deposition. The deposition rate was 0.5 Å/s, as calibrated by a crystal thickness monitor placed at the substrate location prior to deposition. The XRD image shown in Fig. 9 confirms the crystallinity of niobium films by the two observed Nb diffraction orders (110 and 211).

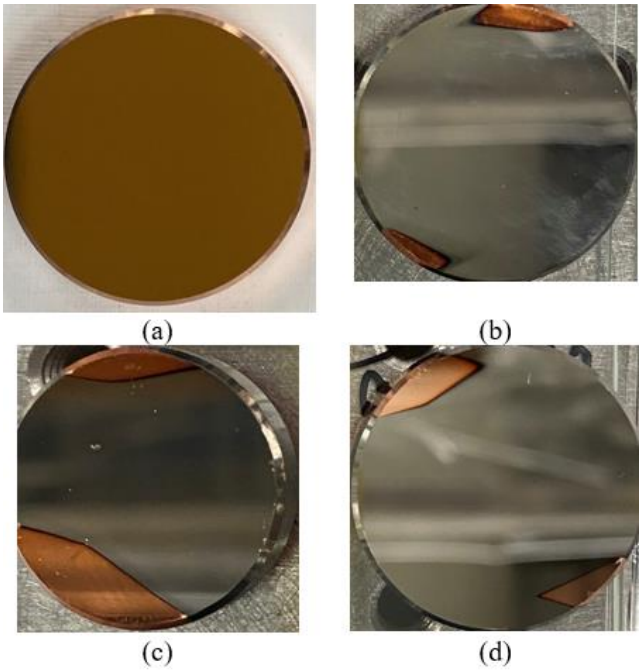

Fig. 8. Cu substrate and sputter-deposited Nb films of varying thicknesses (a) II-VI Cu substrate, (b) 800 nm Nb, (c) 400 nm Nb and (d) 200 nm Nb films on Cu

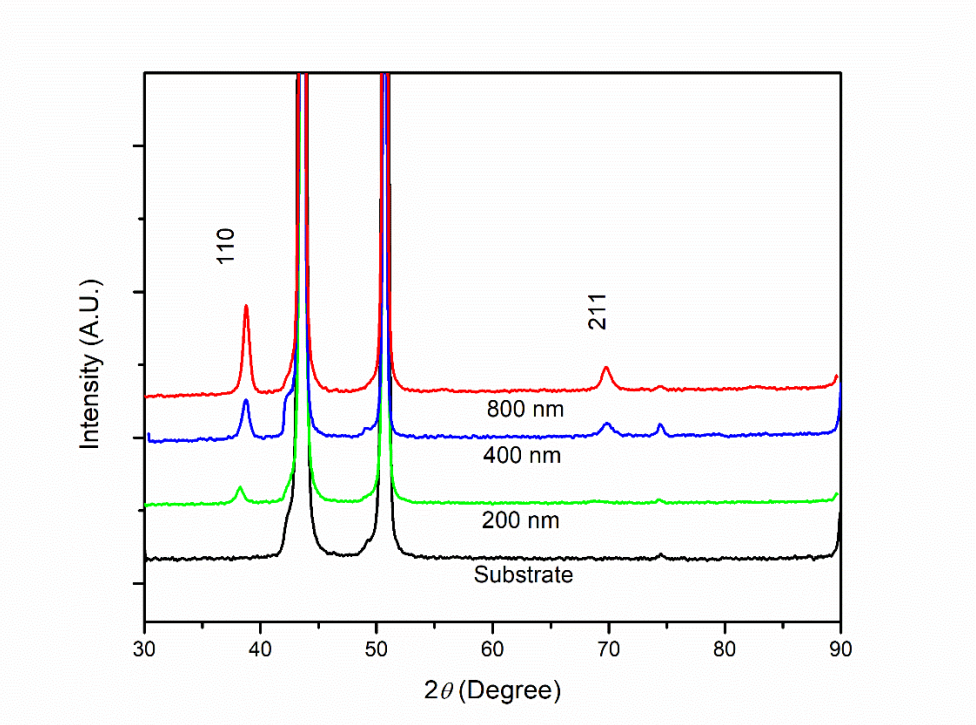

Fig. 9. XRD Image of Cu substrate (black) and Nb films of 200 nm (red), 400 nm (blue) and 800 nm (green) confirms the crystallinity of Nb films.

TDTR scans were obtained for 200, 400, 800 nm Nb films on Cu substrates. The data were taken at room temperature over 0-900 ps time delay between the pump and probe pulses with a scan step of 0.667 ps. To determine the thermal conductivity k, temperature profile for k = 55 $Wm^{-1}K^{-1}$ (conductivity value for bulk Nb) is obtained first and multiplied by a constant that matches the magnitude of the thermoreflectance data and then the value of k has been incremented or decremented by 1 and each time multiplied by an appropriate constant value to achieve the best fitting k value. All data were averaging over 5 scans to avoid noise and FFT filtering were done for clear appearance of acoustic bumps.

A. Measurement of Thermal Conductivity for Nb films of different thickness

Figure 10 portrays the thermal response obtained from Nb film of three different thicknesses: 200 nm, 400 nm and 800 nm deposited on Cu substrate. It is seen that, unlike noble metals like Cu and Au, fermi-level smearing is not observed in our experiment on Nb, only a slow decay component on the order of nano-second was observed. For the Fermi-level smearing to be observed, an inter-band transition has to be excited by the pump photon, involving either an initial or a final electron state close to the Fermi level [9]. Fermi-level smearing depends on the photon energy of the incident beam and fermi energy of the material. The absence of fermi smearing induced by incident photon energy (1.553 eV) on experimental TDTR signals indicates the higher fermi energy of Nb compared to Cu and Au [3].

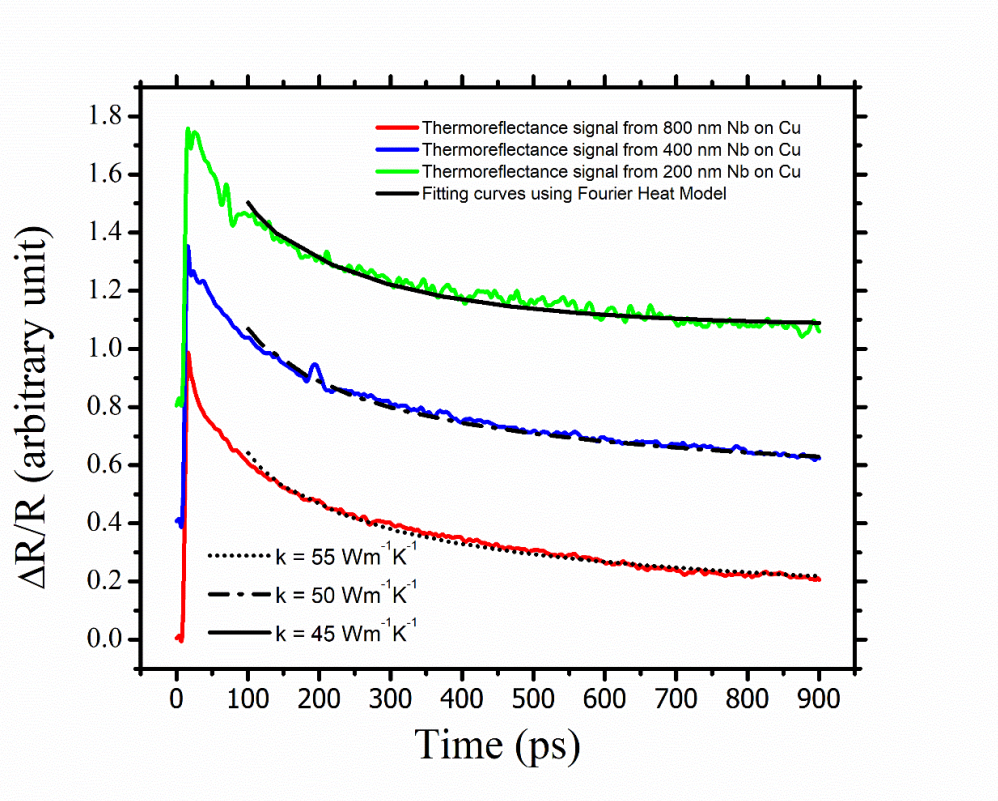

Fig. 10. Thermoreflectance data from Nb samples of three different thicknesses: TDTR signal from 200 nm Nb on Cu (green) fitted with k = 45 Wm-1K-1, from 400 nm Nb on Cu (blue) fitted with k = 50 Wm-1K-1 and from 800 nm Nb on Cu (red) fitted with k = 55 Wm-1K-1. The data in Y axis are shown in arbitrary unit as the normalized data for blue and green curves are shifted by 0.4 and 0.8 units respectively along the positive Y axis.

From Figure 10, it is seen that, thermal conductivity for 800 nm film (k = 55 Wm-1K-1) is obtained same as that of bulk Nb. Thermal conductivity reduces slightly as the thickness decreases from 800 nm to 200 nm. The conductivity values for 400 nm (50 $Wm^{-1}K^{-1}$) and 200 nm (45 $Wm^{-1}K^{-1}$) films are obtained a bit less than that of bulk Nb. This variation of conductivity with Nb film thickness supports the observation by T. Q. Qiu et al. that, for films with thickness much higher than the radiation penetration depth, electrons can carry the absorbed energy away from the radiation absorption region rapidly, resulting in a more rapid surface temperature drop [16]. This small change in thermal conductivity with Nb film thickness can also be verified by the change in grain size of the Nb films which are calculated from the XRD image shown in Fig. 9 using Scherrer equation. The crystallite size of two observed Nb diffraction orders (110 and 211) calculated are presented on table 2. As the film thickness increases the grain size also increases although the change is not so big.

Table 2: Measured crystallite size for Nb films of various thickness

Film Thickness (nm)	Crystallite Size (nm) for diffraction order 110	Crystallite Size (nm) for diffraction order 211
200	15	-
400	16.1	6.0
800	18.5	10.1

B. Effect of Substrates on thermal response

Thermal response may differ for same material deposited on different substrates. This is because substrates play significant role on grain size and crystallinity of the sample. For example, the grain size of Au film deposited on Si substrate is 35 nm whereas it is about 45 nm for Au film on glass substrate [3]. Figure 11 presents the experimentally observed TDTR signals for 400 nm films deposited on two different substrates: sapphire (orange) and Cu (blue) along with the appropriate fitting curves. For 400 nm Nb film with sapphire as substrate has thermal conductivity value similar to the bulk Nb. For Nb film of same thickness, thermal conductivity reduces when Cu is used as substrate compared to sapphire being used as substrate. It can be deduced from here that, although thermal conductivity of copper (401 $Wm^{-1}K^{-1}$) [20] is 10 times higher compared to conductivity value of sapphire (40 $Wm^{-1}K^{-1}$) [22], it induces comparatively less thermal diffusion when used as substrate for Nb films. This obviously reflects the demand for more study on the interface of niobium film with substrate. Interface conductance of Cu-Nb multilayers increases with decreasing layer thickness since the ballistic transport of electrons from Cu-side dominates the thermal conduction due to long mean free path of copper electrons [4]. The sapphire substrate we used to deposit niobium film was highly pure with mirror polished smooth surface leading to Nb film with good quality surface having less defects compared to films deposited on copper substrate.

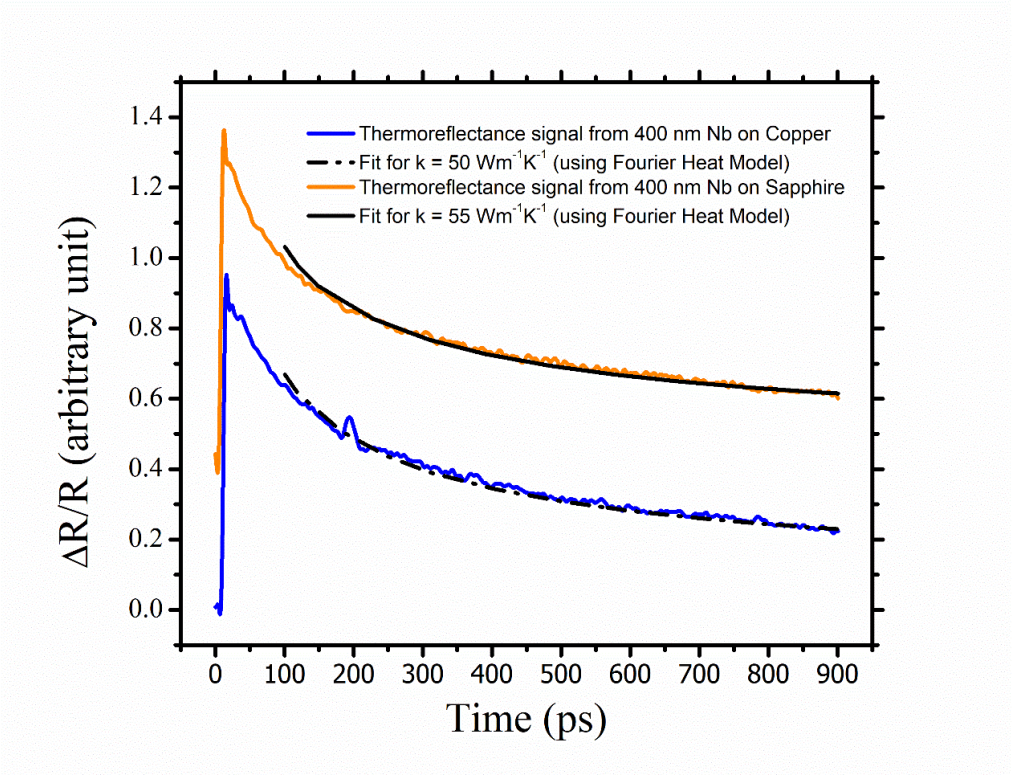

Fig. 11. Thermoreflectance data from 400 nm Nb samples on two substrates: TDTR signal from Nb film on copper (blue curve) fitted with k = 50 W $m^{-1}K^{-1}$ and TDTR signal from Nb film on sapphire (orange curve) fitted with k = 55 W $m^{-1}K^{-1}$. The data in Y axis are shown in arbitrary unit as the normalized data for the orange curve are shifted by 0.4 unit along the positive Y axis.

C. Observation of Acoustic Oscillations on Thermal Response from Nb Films

Absorption of the laser causes thermal expansion and generates acoustic waves of ultrasonic frequency. This strain effects on reflectivity is superimposed with the reflectance due to temporal relaxation profile. These strain effects can be significant depending on the material's thermal expansion, the photon energy, and the fluence of the heating beam [3]. The strain can be divided into two parts. A time-independent strain due to thermal expansion. The second part of the strain is a pulse which propagates away from the free surface at the speed of longitudinal sound. The width of this pulse is of the order of twice the absorption length. After propagating across the film, the pulse will be reflected at the boundary with the substrate and returns to the front surface after a time $t=2d/v$, where d is the thickness of the film and v is the longitudinal sound velocity.

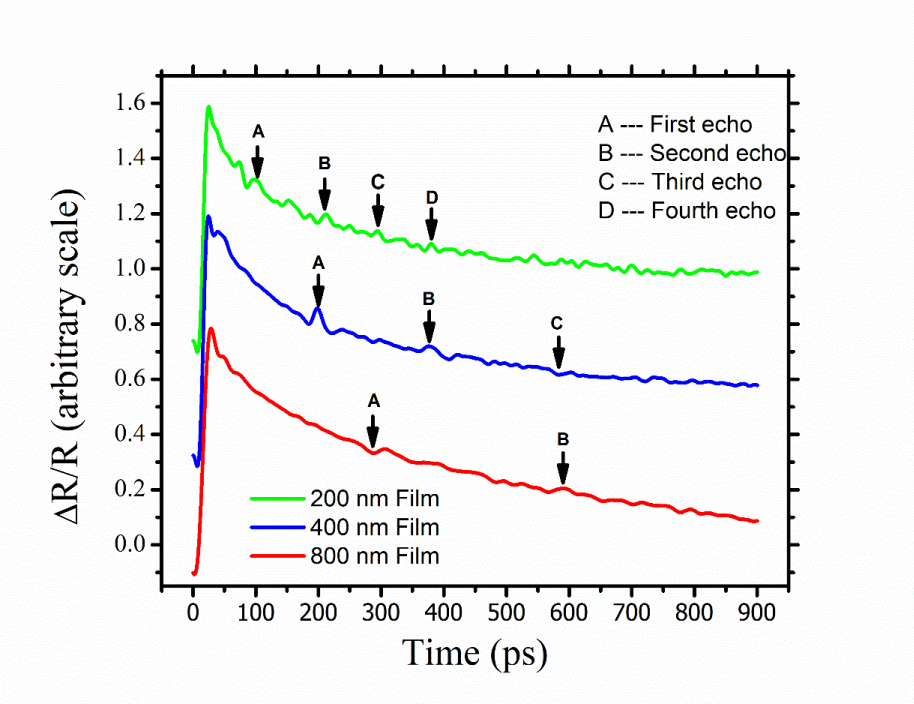

Fig.12. Thermoreflectance curves showing acoustic echoes from 200, 400 and 800 nm Nb on Cu substrate.

Figure 12 shows that, thermoreflectance data containing information about acoustic oscillations measured from Nb films of three different thicknesses. The period of the experimentally observed oscillations varied linearly with the film thickness. Thermoreflectance data obtained from 400 nm Nb film on sapphire substrate do not show any bump which can be consider significantly to measure strain effect, whereas data obtained from niobium films deposited on copper substrate show clear acoustic oscillations with period consistent with the thicknesses of films. Therefore, it can be deduced that, substrates can play significant role in collecting acoustic information from thermal response and the copper substrate from II-VI is a very good choice for this purpose. C. Thomsen observed acoustic echoes in metals with high thermal diffusion like Cu, Al and Ni but they did not find any echo for metals of comparatively lower thermal diffusion such as Mg, Zn, Mo and Sn [23]. Although Nb has much lower thermal diffusion rate compared to Cu, Al and Ni,

acoustic echoes observed potentially because of its higher thermal expansion coefficient and higher acoustic reflection coefficient.

This acoustic information can be used to measure unknown parameters like film thickness or longitudinal sound velocity inside the film if any one of these parameters is known. Figure 13 shows that, thermoreflectance data containing information about acoustic oscillations measured from 400 nm Nb film deposited on Cu substrate. For 400 nm film the period is measured as 182 ps. Using this value of period (t = 182 ps) and film thickness (d = 400 nm) the longitudinal sound velocity (v =2d/t) inside Nb is calculated as 4395.6 ms^{-1}. Our calculated value of longitudinal sound velocity in Nb agreed well with the value (3480-4900 ms^{-1}) reported by Igor L. Shabalin [24].

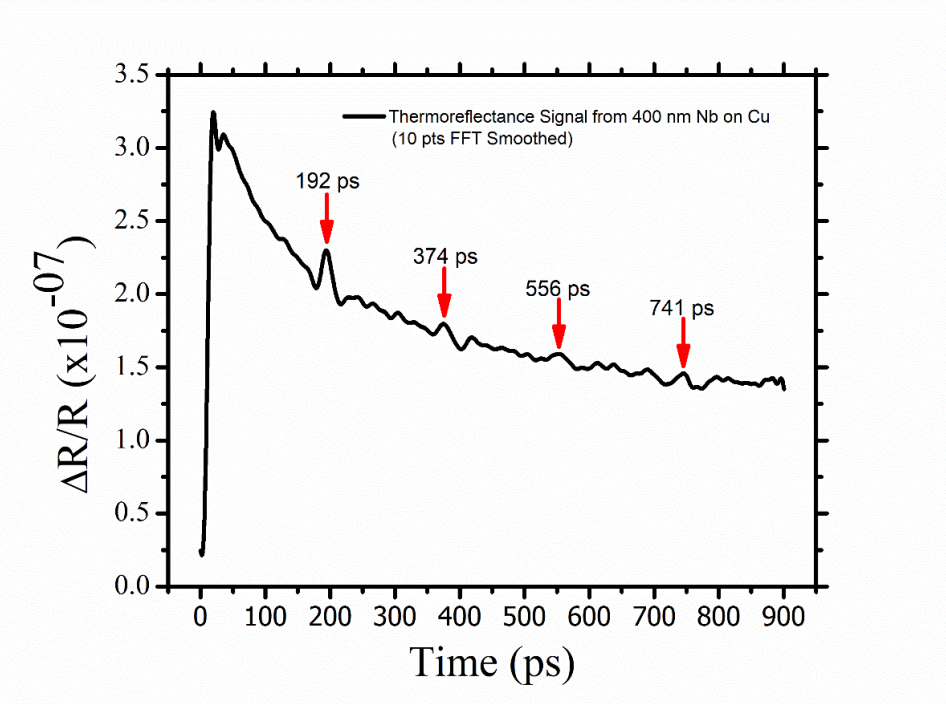

Fig. 13: TDTR signal from 400 nm Nb film on Cu shows acoustic echoes at regular interval. Period of this acoustic oscillations is measured to determine longitudinal sound velocity.

6. Measurement in Thin Niobium Films Deposited at 670^0 C

Niobium films of thickness same as previously deposited films at room temperature (800 nm, 400 nm and 200 nm) were produced using AJA ATC Orion 5 Magnetron sputtering system. But this time the deposition temperature was set to 670^0 C. All the deposition parameters remained same and when the deposition chamber was evacuated to a base pressure of low 10^{-7} Torr the copper substrate was heated to 670^0 C for min before starting the deposition. After film growth, the sample was cooled down to 40^0 C per minute to make sure not to create too much stress between Cu and Nb. The XRD image shown in Fig. 14 confirms the crystallinity of niobium films by the three observed Nb diffraction orders (110, 200 and 220).

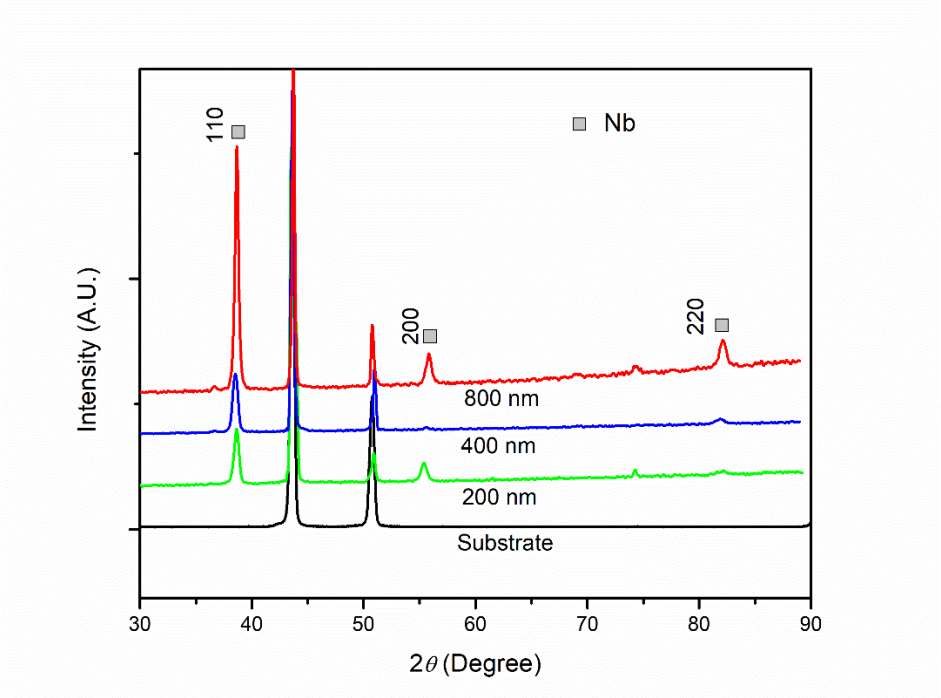

Fig. 14. XRD Image of Cu substrate (black) and Nb films of 200 nm (red), 400 nm (blue) and 800 nm (green) confirms the crystallinity of Nb films.

A. Measurement of Thermal Conductivity for Nb films of different thickness

Figure 15 (a) displays the thermal response obtained from Nb film of three different thicknesses (200 nm, 400 nm and 800 nm) deposited on Cu substrate at 670^0 C. It is seen that thermal response from 800 nm and 400 nm films are similar and overlapping but response from 200 nm is different than that obtained from other two films. Figure 15 (b) shows the thermoreflectance curves fitted with 1D Heat Model. Thermal conductivity for 800 nm and 400 nm films ($k = 55\ Wm^{-1}K^{-1}$) is obtained same as that of bulk Nb and it is obtained 50 $Wm^{-1}K^{-1}$ for 200 nm films. This result indicates the conductivity dependance on film structure that changes with film thickness as well as deposition temperature. The crystallite size of Nb films of different thicknesses deposited bot at room temperature and 670^0 C for diffraction orders 110 calculated from the XRD images using Scherrer equation are presented on table 3. The grain size of Nb films increases with film thickness and deposition temperature.

Table 3: Measured crystallite size for Nb films of various thickness deposited at 670^0 C

Film Thickness (nm)	Crystallite Size (nm) for diffraction order 110	
	Room Temperature Deposition	Deposition at Temperature 670^0 C
200	15	17.5
400	16.1	17.4
800	18.5	32.0

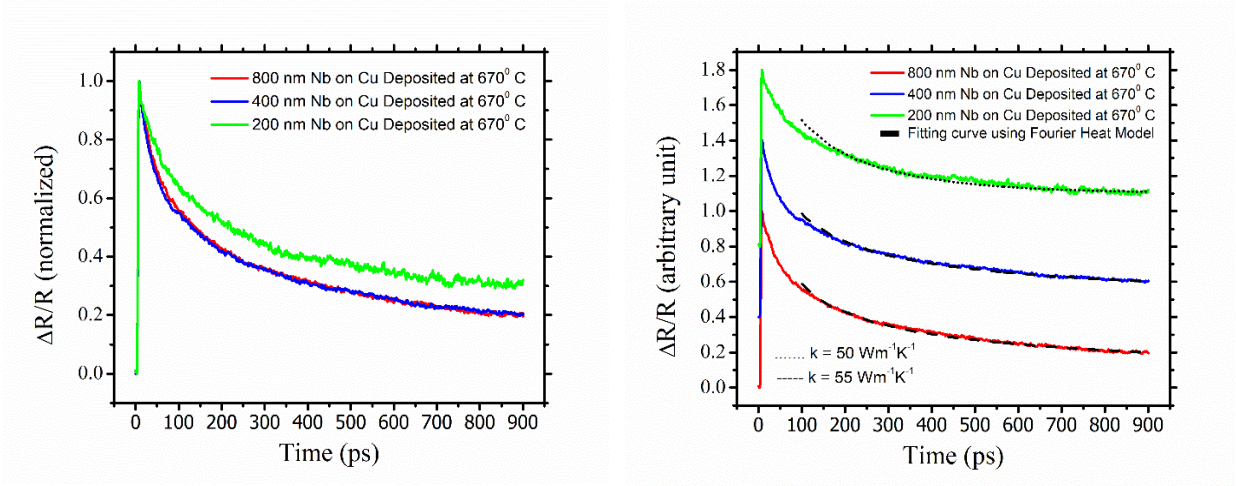

(a) (b)

Fig. 15. (a) Thermoreflectance data (normalized) from Nb samples of three different thicknesses deposited at temperature 670^0 C. (b) TDTR signal from 200 nm Nb on Cu (green) fitted with k = 50 Wm-1K-1, from 400 nm Nb on Cu (blue) and from 800 nm Nb on Cu (red) fitted with k = 55 Wm-1K-1. The data in Y axis are shown in arbitrary unit as the normalized data for blue and green curves are shifted by 0.4 and 0.8 units respectively along the positive Y axis.

B. Effect of Deposition Temperature on thermal response

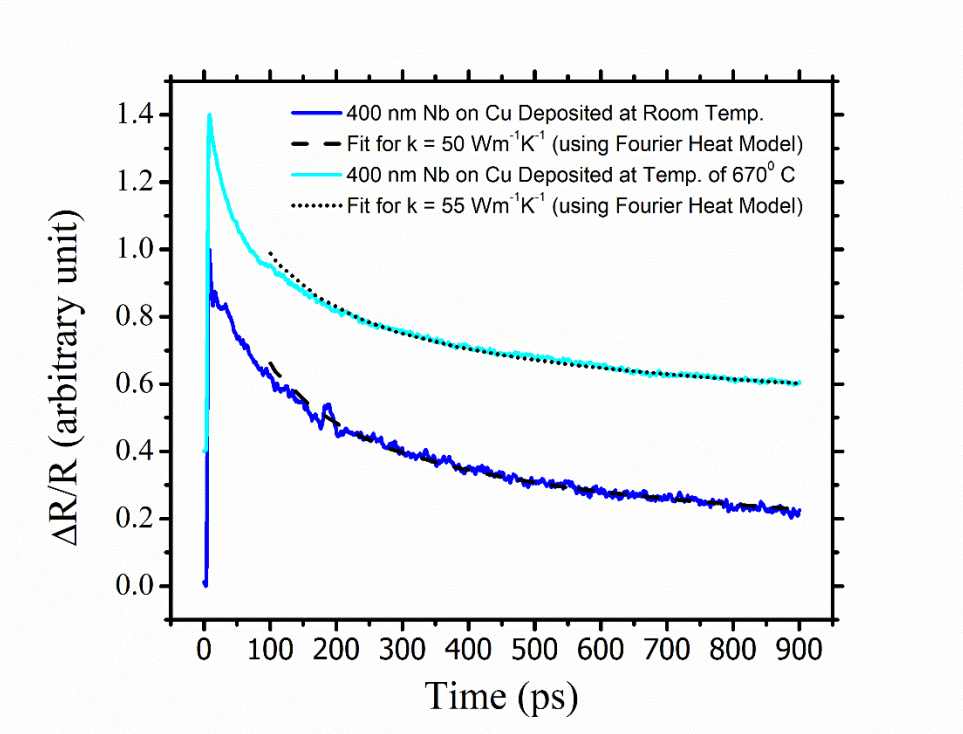

Fig. 16. Thermoreflectance data from 400 nm Nb samples on two substrates: TDTR signal from Nb film on copper (blue curve) fitted with k = 50 W $m^{-1}K^{-1}$ and TDTR signal from Nb film on sapphire (orange curve) fitted with k = 55 W $m^{-1}K^{-1}$. The data in Y axis are shown in arbitrary unit as the normalized data for the orange curve are shifted by 0.4 unit along the positive Y axis.

Figure 16 displays the thermal responses observed for 400 nm Nb films deposited on Cu at different temperatures: room temperature (blue curve) and 670^0 C (cyan curve). The conductivity fitting using Fourier Heat Model depicts the effect of deposition temperature on thermal diffusion. 400 nm Nb film deposited at room temperature gives lower thermal conductivity ($k = 50\ Wm^{-1}K^{-1}$) than bulk Nb ($k = 55\ Wm^{-1}K^{-1}$) but the thermal conductivity on 400 nm film deposited at higher temperature (670^0 C) matched well with that of bulk Nb. Therefore, for thin film deposition, it is highly recommended to deposit Nb on Cu at temperature as high as possible. Deposition at high temperature may cause surface roughness but high temperature deposition of Nb on Cu is also recommended as it results for sharper critical temperature transition which is very important in implementing Nb coated Cu SRF cavities [15]. Deposition temperature is therefore a critical concern in growing Nb on Cu.

7. Conclusion

Thermal response of bulk niobium and Nb films of three different thicknesses deposited at room temperature and 670^0 C is measured by pump-probe femtosecond thermo-modulation spectroscopy to investigate the effect of film thickness, substrate and deposition temperature on thermal diffusion using the parabolic one step Fourier's heat conduction model. Thermal measurement in bulk Nb on different spots of the sample investigated that the variation of thermal conductivity for different scans is about $\pm$ 1 $Wm^{-1}K^{-1}$.

Reduction in thermal conduction with decreasing film thickness for 800, 400, 200 nm films on Cu substrate deposited at room temperature is observed. The thermal conductivity of 800 nm and 400 nm Nb films deposited at 670^0 C is measured same as that of bulk niobium, but it is measured a bit less for the 200 nm film deposited at same temperature. Therefore, higher deposition temperature is needed for thin Nb films deposited on Cu for better thermal diffusion. Since Nb films deposited on sapphire with thickness (400 nm) same as on the Cu gives better thermal conductivity and increasing deposition temperature improve conductivity, deposition temperature is very crucial in growing Nb on copper.

The thermal response shows clear acoustic bumps due to strain effect which is used here in measuring the longitudinal sound velocity inside Nb film with known film thickness. The value calculated for longitudinal sound velocity inside niobium is 4395.6 ms^{-1}, which is within the range (3480-4900 ms^{-1}) reported in literature [20]. Having comparatively lower thermal diffusion rate of Nb than noble metals like (Au, Cu, Ag etc.) the clear and regularly spaced acoustic bumps observed on experimental thermal response indicates higher thermal expansion coefficient and higher acoustic reflection coefficient of niobium.

II-VI Cu Samples Utilization:

Total 10 piece of copper samples were obtained from II-VI. Among these 10 sample 4 were used for depositing Nb at room temperature: one for 800 nm, one for 400 nm and other two for 200 nm films (one 200 nm sample did not give TDTR data). Three other pieces are used for depositing Nb of same thickness but at high temperature (670^0C) to improve the crystallinity of films and then measure thermoreflectance by pump-probe technique. One piece was used for XRD analysis as background and the other two remain unused. All the thermoreflectance data taken till date are at room temperature. To measure thermal spectroscopy at low temperature, a new cryogenic system is setting up but due to the recent corona virus pandemic and limited access to lab the installation process has not been completed yet.

References:

[1]. H. Padamsee, The science and technology of superconducting cavities for accelerators, Supercond. Sci. Technol. 14 (2001) R28–R51.

[2]. L. Catani, A. Cianchi, D. Di Giovenale, J. Lorkiewicz, V. Merlo, R. Polini, C. Granata, R. Russo, M.J. Sadowski, M. Salvato, P. Strzyzewski, S. Tazzari, "Deposition and Characterisation of Niobium Films for SRF Cavity Application," in Proc. EUROCON 2007 - The International Conference on "Computer as a Tool", Warsaw, Poland, Sept. 2007, pp. 1170-1177.

[3]. J. L. Hostetler, A. N. Smith, D. M. Czajkowsky, and P. M. Norris, Measurement of the electron-phonon coupling factor dependence on film thickness and grain size in Au, Cr, and Al, Appl. Opt., 38 (1999) 3614-3620.

[4]. R. Cheaito, J. C. Duda, T. E. Beechem, D. L. Medlin, K. Hattar, E. S. Peikos, A. Misra, J. K. Baldwin, P. E. Hopkins, "The effect of ballistic electron transport on copper-niobium thermal interface conductance," in Proc. ASME Summer Heat Transfer Conference (HT2013), Minnesota, USA, Jul. 2013, pp. 1-5.

[5]. K.M. Yoo, X.M. Zhao, M. Siddique, R.R. Alfano, D.P. Osterman, M. Radparvar, J. Cunniff, Femtosecond thermal modulation measurements of electron-phonon relaxation in niobium, Appl. Phys. Lett., 56 (1990) 1908-1910.

[6]. G.L. Eesley, Observation of Nonequilibrium Electron Heating in Copper, Phys. Rev. Lett., 51 (1983) 2140-2143.

[7]. H.E. Elsayed-Ali, T.B. Norris, M.A. Pessot, G.A. Mourou, Time-resolved observation of electron-phonon relaxation in copper, Phys. Rev. Lett., 58 (1987) 1212-1215.

[8]. R.W. Schoenlein, W.Z. Lin, J.G. Fujimoto, G.L. Eesley, Femtosecond studies of nonequilibrium electronic processes in metals, Phys. Rev. Lett., 58 (1987) 1680-1683.

[9]. M. Mihailidi, Q. Xing, K.M. Yoo, R.R. Alfano, Electron-phonon relaxation dynamics of niobium metal as a function of temperature, Phys. Rev. B, 49 (1994) 3207-3212.

[10]. M. Mihailidi, R.R. Alfano, Time dependence of the electron-phonon coupling parameter of niobium, Appl. Phys. Lett., 65 (1994) 106-108.

[11] C.A. Paddock, G.L. Eesley, Transient thermoreflectance from thin metal films, J. Appl. Phys., 60 (1986) 285-290.

[12]. R. Cheaito, C.S. Gorham, A. Misra, K. Hattar, P.E. Hopkins, Thermal conductivity measurements via time-domain thermoreflectance for the characterization of radiation induced damage, J. Mater. Res., 30 (2015) 1403-1412.

[14]. B. L. Altshuler, A. G. Aronov, D. E. Khmelnitsky, Effects of electron-electron collisions with small energy transfers on quantum, Journal of Physics C: Solid State Physics, 15, 36 (1982) 7367.

[15]. A. Schmid, Electron-phonon Interaction in an Impure Metal, Z. Phys., 259 (1973) 421-436.

[16]. W. M. Roach, D. B. Beringer, J.R. Skuza, W. A. Oliver, C. Clavero, C. E. Reece, R. A. Lukaszew, Niobium thin film deposition studies on copper surfaces for superconducting radio frequency cavity applications, PHYSICAL REVIEW SPECIAL TOPICS - ACCELERATORS AND BEAMS 15, (2012) 062002.

[16]. T. Q. QIU, T. JUHASZ, C. SUAREZ, W. E. BRONS and C. L. TIEN, Femtosecond laser heating of multi-layer metals-II. Experiments, Int. J. Heat Mars Trans, 37 (1994) 2799-2808.

[17]. T. Q. QIU, and C. L. TIEN, Femtosecond laser heating of multi-layer metals-I. Experiments, Int. J. Heat Mars Trans, 37 (1994) 2789-2797.

[18]. T. Q. Qiu and C. L. Tien, Heat Transfer Mechanism During Short-Pulse Laser Heating on Metals, Int. J. Heat Mass Transfer, 35 (1992) 719-725.

[19]. J.K. Chen, J.E. Beraun, Numerical study of ultrashort laser pulse interactions with metal films, Numer. Heat Transfer A, 40 (2001) 1–20.

[20]. J. Hohlfeld, S. S. Wellershoff, J. Gudde, U. Conrad, V. Jahnke, and E. Matthias, Electron and Lattice Dynamics Following Optical Excitation of Metals, Chemical Phys., 251 (2000) 237-258.

[21]. F. Koechlin, B. Bonin, Parametrization of the niobium thermal conductivity in the superconducting state, Superconductor Science and Technology, 9 (1996) 453.

[22]. D. G. Cahill, S.-M. Lee, and T. I. Selinder, Thermal conductivity of k-Al_2O_3 and α-Al_2O_3 wear-resistant coatings, J. Appl. Phys., 83 (1998) 5783-5786.

[23]. C. Thomsen, H. T. Grahn, H. J. Maris, and J. Tauc, Surface generation and detection of phonons by picosecond light pulses, Phys. Rev. B, 34 (1986) 4129-4138.

[24]. I. L. Shabalin, "Niobium," Ultra-High Temperature Materials I: Carbon (Graphene/Graphite) and Refractory Metals, Dordrecht, Netherlands, Springer, 2014, ch. 8, sec. 8.4, pp. 539. [online]. Available: https://link.springer.com/book/10.1007/978-94-007-7587-9

Appendix A

Fourier Heat Conduction Model

The heat equation governs the temperature distribution in an object. Consider the temperature in a 1-D bar of length L (the bar starts off at x = 0 and ends when we reach x = L) At any location, x the temperature will be constant at every point in the cross section at that x. If we assume that the lateral surface of the bar is perfectly insulated (i.e. no heat can flow through the lateral surface) then the only way heat can enter or leave the bar as at either end. This means that heat can only flow from left to right or right to left and thus creating a 1-D temperature distribution.

Some definitions related to the heat equation:

u (x, t) is the Temperature at any point, x and any time, t.

c (x): specific heat is the amount of heat energy that it takes to raise one unit of mass of the material by one unit of temperature [$c\ (x) > 0$]. The specific heat may not be uniform throughout the bar and in practice the specific heat depends upon the temperature. However, this will generally only be an issue for large temperature differences.

ρ(x): mass density is the mass per unit volume of the material, may not be uniform throughout the bar.

Φ (x, t): heat flux is the amount of thermal energy that flows to the right per unit surface area per unit time. The "flows to the right" bit simply tells us that if $\phi\ (x, t) > 0$ for some x and t then the heat is flowing to the right at that point and time. Likewise, if $\phi\ (x, t) < 0$ then the heat will be flowing to the left at that point and time.

Q (x, t): heat energy generated per unit volume per unit time. If $Q(x,\ t) > 0$ then heat energy is being added to the system at that location and time and if $Q(x,\ t) < 0$ then heat energy is being removed from the system at that location and time.

With these quantities the heat equation is,

$$C_p(x)\rho(x)\frac{\partial u}{\partial t} = -\frac{\partial \varphi}{\partial x} + S(x,t) \dots\dots\dots\dots\dots\dots\dots\dots\dots\dots\dots\dots\dots\dots\dots (A1)$$

In this form there are two unknown functions, u and ϕ, and so we need to get rid of one of them. With **Fourier's law** we can easily remove the heat flux from this equation. Fourier's law states that,

$$\varphi(x,t) = -K_0(x)\frac{\partial y}{\partial x} \dots\dots\dots\dots\dots\dots\dots\dots\dots\dots\dots\dots\dots\dots\dots\dots (A2)$$

where $K_0(x)$ [> 0] is the **thermal conductivity** of the material and measures the ability of a given material to conduct heat. The thermal conductivity can vary with the location in the bar and with temperature. But we will assume that the total temperature change is not so great so we will assume for the purposes here that the thermal conductivity will not vary with temperature.

So, if we plug Fourier's law into (1), we get the following form of the heat equation,

$$C_p(x)\rho(x)\frac{\partial u}{\partial t} = \frac{\partial}{\partial x}\left(K_0(x)\frac{\partial u}{\partial x}\right) + S(x,t) \ldots\ldots\ldots\ldots\ldots\ldots\ldots\ldots\ldots\ldots (A3)$$

Solving (2) is quite difficult due to the non-uniform nature of the thermal properties and the mass density. So, let's now assume that these properties are all constant, *i.e.*,

$$C_p(x) = C_p \qquad \rho(x) = \rho \qquad K_0(x) = K_0$$

In this case we generally say that the material in the bar is **uniform**. Under these assumptions the heat equation becomes,

$$\rho C_p \frac{\partial u}{\partial t} = K_0 \frac{\partial^2 u}{\partial x^2} + S(x,t) \ldots\ldots\ldots\ldots\ldots\ldots\ldots\ldots\ldots\ldots (A4)$$

In case where the source is a LASER and the heat energy generated per unit volume is given by,

$$S(x,t) = (1-R)I\alpha * \exp\left[-\alpha x - 2.77\left(\frac{t}{t_p}\right)^2\right] \ldots\ldots\ldots\ldots\ldots\ldots\ldots\ldots (A5)$$

Where, R is the reflectivity of the material on which laser incident t_p is laser pulse width and I is the intensity of the laser pump given by

$$I = \frac{Pulse\ energy}{Pulse\ cross\ section\ \times\ pulse\ width} \ldots\ldots\ldots\ldots\ldots\ldots\ldots\ldots (A6)$$

Using MATLAB built-in function "pdepe" the heat equation can be solved. The pdepe solves three equations one for function (A7), one for initial condition (A8) and the rest is for boundary conditions (A9).

$$c\left(x,t,u,\frac{\partial u}{\partial x}\right)\frac{\partial u}{\partial t} = x^{-m}\frac{\partial}{\partial x}\left(x^m f\left(x,t,u,\frac{\partial u}{\partial x}\right)\right) + S\left(x,t,u,\frac{\partial u}{\partial x}\right) \ldots\ldots\ldots\ldots (A7)$$

$$u(x,t_0) = u_0(x) \ldots\ldots\ldots\ldots\ldots\ldots\ldots\ldots\ldots\ldots\ldots\ldots (A8)$$

$$p(x,t.u) + q(x,t)\, f\left(x,t,u,\frac{\partial u}{\partial x}\right) = 0 \ldots\ldots\ldots\ldots\ldots\ldots\ldots\ldots\ldots (A9)$$

Where, m = 0 for cartesian, 1 for cylindrical and 2 for spherical coordinate system. The initial condition is the initial temperature which is set to the room temperature (300 K) and during the short period of laser heating, heat losses from the front and back surfaces of the film can be neglected, leading to the thermal-insulation boundary conditions. At the front end (x = 0), pl = 0 and ql = 1 and at the back surface (x = L), pr = 0 and qr = 1.

MATLAB CODE:

```
function parabolic
L=1000E-9;      %m
tend=1000E-12; %seconds

m = 0;
x = linspace(0,L,1000);
t = linspace(-415E-15,tend,2000);

sol = pdepe(m,@pdex5pde,@pdex5ic,@pdex5bc,x,t);
u = sol(:,:,1);
xlswrite('C:\Users\obidu\OneDrive\Desktop\matlab
example\test1.xls',t(:));
xlswrite('C:\Users\obidu\OneDrive\Desktop\matlab
example\test1.xls',u,'b1:b2000');

% A surface plot is often a good way to study a solution.
%surf(x,t,u)
%title('Numerical solution computed with 20 mesh points.')
%xlabel('Distance x')
%ylabel('Time t')

%Plot surface temperature vs. time
%figure, plot(t,u(:,1))
%title('Surface Temperature')
%xlabel('Time (s)')
%ylabel('Temperature (K)')

%Plot surface temperature vs. time
%subplot(3,2,1)
%plot(t,u(:,1))
%title('Temperature Profile at the front surface')
%xlabel('Time (s)')
%ylabel('Temperature (K)')

%subplot(3,2,2)
%plot(t,u(:,2))
%title('Temperature Profile at x = 20 nm')
%xlabel('Time (s)')
%ylabel('Temperature (K)')

%subplot(3,2,3)
%plot(t,u(:,5))
```

```
%title('Temperature Profile at x = 50 nm')
%xlabel('Time (s)')
%ylabel('Temperature (K)')

%subplot(3,2,4)
%plot(t,u(:,10))
%title('Temperature Profile at x = 100 nm')
%xlabel('Time (s)')
%ylabel('Temperature (K)')

%subplot(3,2,5)
%plot(t,u(:,20))
%title('Temperature Profile at x = 200 nm')
%xlabel('Time (s)')
%ylabel('Temperature (K)')

%subplot(3,2,6)
%plot(t,u(:,50))
%title('Temperature Profile at x = 500 nm')
%xlabel('Time (s)')
%ylabel('Temperature (K)')

% A solution profile can also be illuminating.
subplot(3,2,1)
plot(x,u(1,:))
title('Spatial Temp. Prof. at time of pump heating')
xlabel('Distance x (um)')
ylabel('Temperature (K)')

subplot(3,2,2)
plot(x,u(2,:))
title('Spatial Tem. Prof. at t = 1 ps')
xlabel('Distance x (um)')
ylabel('Temperature (K)')

subplot(3,2,3)
plot(x,u(100,:))
title('Spatial Tem. Prof. at t = 50 ps')
xlabel('Distance x (um)')
ylabel('Temperature (K)')

subplot(3,2,4)
plot(x,u(200,:))
title('Spatial Tem. Prof. at t = 100 ps')
```

```
xlabel('Distance x (um)')
ylabel('Temperature (K)')

subplot(3,2,5)
plot(x,u(1000,:))
title('Spatial Tem. Prof. at t = 500 ps')
xlabel('Distance x (um)')
ylabel('Temperature (K)')

subplot(3,2,6)
plot(x,u(2000,:))
title('Spatial Tem. Prof. at t = 1 ns')
xlabel('Distance x (um)')
ylabel('Temperature (K)')
end


function [c,f,s] = pdex5pde(x,t,u,DuDx)
c = 2.3E6;
f = 55*DuDx;
s = ((1-0.9)*3.98/(100E-15*15.3E-9))*exp(-(x/15.3E-9)-
(2.77*(t/100E-15)^2));
end

function u0 = pdex5ic(x)
u0 = 300;
end

function [pl,ql,pr,qr] = pdex5bc(xl,ul,xr,ur,t)
pl = 0;
ql = 1;
pr = 0;
qr = 1;
end
```

Temperature Profile of 1 µm Nb film at the front surface:

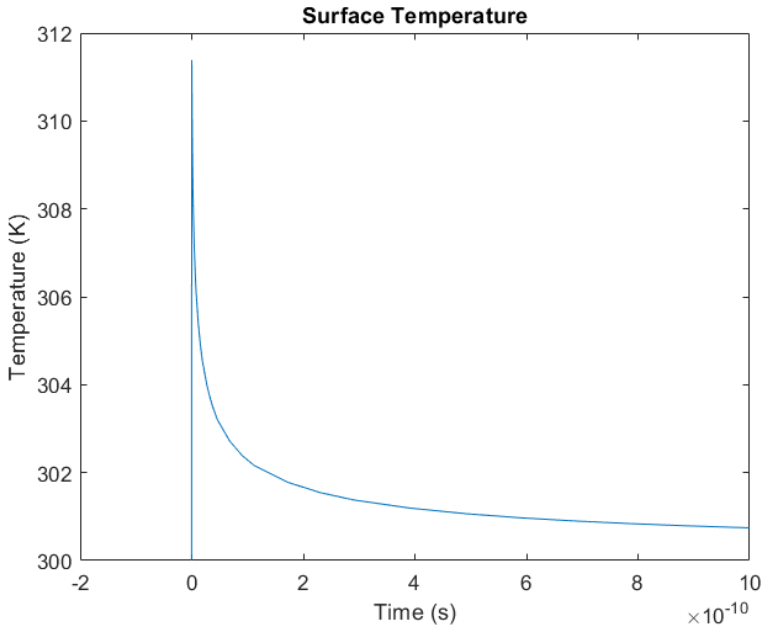

Temperature Profile of 1 µm Nb film at different spatial position:

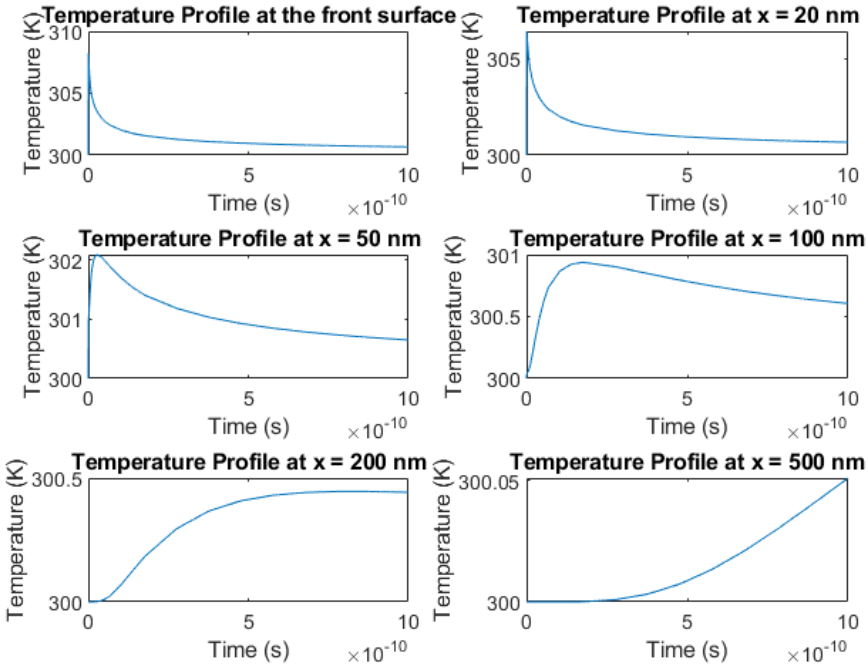

Spatial Temperature Profile of 1 µm Nb film at different time instants: